CHEMISTRY OF MATERIALS

Article

pubs.acs.org/cm

Controlling the Relative Areas of Photocathodic and Photoanodic Terraces on the $SrTiO_3(111)$ Surface

Yisi Zhu, Paul A. Salvador, and Gregory S. Rohrer*

Department of Materials Science and Engineering, Carnegie Mellon University, Pittsburgh, Pennsylvania 15213, United States

Supporting Information

ABSTRACT: $SrTiO_3(111)$ surfaces have been heated in air at 1250 °C, either alone or with reservoirs of TiO_2 and $SrTiO_3$ powders. The surface structure and properties were measured by atomic force microscopy, scanning Kelvin probe microscopy, X-ray photoelectron spectroscopy (XPS), and photochemical marker reactions that leave solid products on the surface at the site of the photochemical reaction. All of the surfaces are made up of atomically flat terraces of two distinguishable types. One terrace has a relatively higher surface potential and promotes the photochemical reduction of Ag^+. The other terrace has a relatively lower positive potential and promotes the photochemical oxidation of Pb^{2+}. XPS measurements show that the concentration of titanium at the surface increases with the fraction of TiO_2 in the powder reservoir during annealing, and marker reactions show the fraction of terraces that promote oxidation increases with the titanium content. The fractional area of terraces that promote oxidation was controlled between 45% and 86% of the total area.

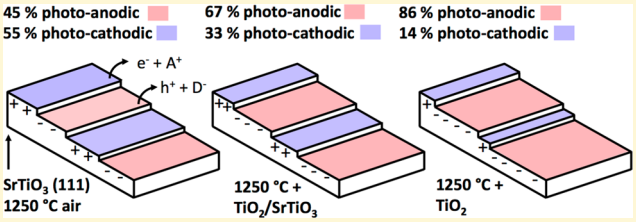

1. INTRODUCTION

Photochemical reactions on semiconductor surfaces have been studied for decades with the goal of developing improved catalysts that can be used to separate hydrogen from water or degrade pollutants.[1−5] However, photocatalytic water-splitting is not yet a commercial technology because of its low efficiency when driven by visible light. Semiconducting oxides are one of the most promising types of photocatalysts because of their relative stability in sunlight and water. For an individual photocatalyst carrying out both photochemical half-reactions, the overall efficiency is limited by the slower of the two half-reactions.[6] Thus, controlling the relative areas of the surface that promote oxidation and reduction is a key to optimizing the overall efficiency of a photocatalyst. Local surface charges can cause an oxide surface to favor either oxidation or reduction. For example, at the surface of ferroelectric oxides, positively charged domains favor reduction and negatively charged domains favor oxidation.[7−9] The separation of electrons and holes to photocathodic and photoanodic sites has also been suggested to increase overall photochemical efficiency by reducing charge carrier recombination and the back reaction.[10−12] Therefore, it is of great interest to develop new methods to control local surface charges that impact local photochemical reactivity.

Here we focus on controlling surface charges on strontium titanate ($SrTiO_3$), a well-known photocatalyst that can split water under UV-light.[13,14] We choose to focus on single crystal (111) surfaces because the bulk truncated (111) surface is polar. Polar surface terminations are created when an ionic crystal is cleaved and the two new surfaces each have a net (and opposite) charge. $SrTiO_3$ crystallizes in the cubic perovskite structure (a = 3.905 Å), as shown in Figure 1a. The unreconstructed $SrTiO_3(111)$ surface is polar because it can

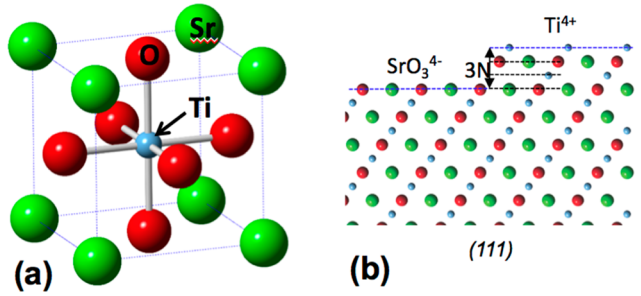

Figure 1. (a) Unit cell of perovskite $SrTiO_3$. (b) Schematic of $SrTiO_3$ viewed along $[1\bar{1}0]$. The dashed lines indicate the (111) planes. Along the [111] direction, $SrTiO_3$ is composed of alternating SrO_3^{4-} and Ti^{4+} atomic layers separated by N = 1.12 Å.

be terminated either by Ti^{4+} or SrO_3^{4-}, as shown in the side view depiction in Figure 1b. The spacing between two atomic layers of different chemical compositions is an odd multiple of N ($N = \sqrt{3}/6a$ = 1.12 Å). For example, the step height between the Ti^{4+} and SrO_3^{4-} layers in Figure 1b is $3N$. Although this "bulk truncation" model is a reasonable starting point, it must be recognized that for samples exposed to air, submerged in aqueous solutions, or annealed at high temperature where diffusion is activated, the real $SrTiO_3(111)$ surface

Received: June 1, 2016
Revised: June 29, 2016
Published: June 30, 2016

DOI: 10.1021/acs.chemmater.6b02205
Chem. Mater. 2016, 28, 5155−5162

is likely to be reconstructed in some way,[15] and will definitely have a layer of adsorbates[16,17] and an associated space charge region.

It has already been shown that distinct terraces on the $SrTiO_3(111)$ surface separately promote reduction and oxidation in photochemical reactions.[18] In other words, one terrace is photocathodic and the other is photoanodic. However, the compositions and potentials of these different surfaces have not yet been measured. According to the results of semiempirical Hartree−Fock method calculations, titanium rich surfaces have a greater work function than strontium rich surfaces by 0.3 to 0.8 eV, depending on the surface composition.[19] Experimental measurements yield smaller differences.[20] In fact, the Ti-rich surface can have a work function that is sometimes greater than and sometimes less than the Sr-rich surface, depending on the way the surface is prepared.[20] In this work, Kelvin probe force microscopy (KFM) is used to measure the difference in the overall surface potential of the terraces with different reactivities. It will be shown that the two terraces have distinct contrast in KFM images, which makes them interact differently with electrons and holes, yielding different reactivities.

In the early work that identified photoanodic and photocathodic terraces on the $SrTiO_3(111)$ surface, it was not clear what determined the relative areas of the two terraces.[18,21] Since then, others have produced surfaces with a uniform Ti-rich termination by thermal annealing in ultra high vacuum[22] or by etching with a buffered hydrogen fluoride solution.[23−25] The goal of creating uniform terminations was to promote improved thin film crystal growth. However, from a photochemical point of view, one would like to tailor the ratio of the two types of terminations to maximize the overall reaction rates by equalizing the net reduction and oxidation rates. In general, the area specific reaction rate (rate per surface area) is not expected to be the same for reactions on different terraces. However, the overall reaction rate could be optimized by creating surfaces with relative areas of the two terraces that are the inverse of their relative area specific reduction and oxidation rates. We describe a novel method to control the relative area of Ti-rich or Sr-rich surfaces, which is generally applicable to their use as photocatalyts and as substrates in thin film growth.

This paper has two main purposes. The first is to expand what we know about the surface potential and chemical composition of the two different terraces on the $SrTiO_3(111)$ surface. The relative surface potentials will be measured by Kelvin probe force microscopy (KFM) and correlated to the relative reactivities measured by photochemical marker reactions and to the step heights between the terraces measured by atomic force microscopy (AFM). Furthermore, by comparing X-ray photoelectron spectra (XPS) of surfaces with different measured potentials and reactivity, we can determine how the reactivity is correlated to the relative concentrations of Sr and Ti on the surface. The second purpose is to show that we can control the fractions of the surface that promote reduction and oxidation. We use a novel method that involves a high temperature anneal in the presence of reservoirs of TiO_2 and $SrTiO_3$ powder mixtures. By increasing the amount of TiO_2 in the powder reservoir, we increase (or decrease) the amount of Ti (or Sr) on the surface. We show here that, by controlling the termination and surface potential distribution, we also control the photochemical properties of the surface, and that these properties are stable with time.

2. EXPERIMENTAL PROCEDURE

Chemical−mechanical polished $SrTiO_3(111)$ single crystals (MTI company, (111) ± 0.5°, roughness < 5 Å) were sonicated in a methanol bath for 10 min and then placed in a covered rectangular alumina combustion boat and annealed in a muffle furnace at 1250 °C for 10 h (ramp rates were 5 °C/min). After annealing, atomically flat terraces, 0.5 to 3 μm wide, were observed by AFM (Solver-Next, NT-MDT, Russia). A set of similar experiments was carried out to test the sensitivity of the surface structure to the annealing environment. In these experiments, the $SrTiO_3(111)$ crystal was put at the center of the same combustion boat and then surrounded by reservoirs of TiO_2 and $SrTiO_3$ powder mixtures with different compositions. The combustion boat was then covered and heated with the schedule described above.

Photochemically generated solid Ag- and Pb-containing reaction products were used to mark the locations of the reduction and oxidation reactions, respectively.[18,26−30] A Viton O-ring (diameter ~0.5 cm) was placed on the annealed $SrTiO_3(111)$ sample surface, aqueous solutions of 0.115 M $AgNO_3$ or $Pb(CH_3COO)_2$ were poured into the O-ring and a quartz slip was placed on top, sealing the solution in the O-ring by capillarity without an air bubble. Next, a 300 W mercury lamp (Newport, Irvine, CA) was used to illuminate the assembly. During this procedure, skin and eyes must be protected to prevent damage by UV radiation. The exposure time was 8 s for Ag^+ reduction and 30 s for Pb^{2+} oxidation. After illumination, the $SrTiO_3(111)$ sample was rinsed with deionized water and dried using a stream of 99.995% nitrogen gas.

Three scanning probe techniques were used to characterize the surface before and after the photochemical reactions. KFM was used to record the local surface potential of each terrace. A silicon AFM probe with a TiN (FMG01/TiN, NT-MDT) or PtCr (190E-G, budget sensor) conductive coating was used for the surface potential measurement. High-precision AFM images were used to measure the step height between neighboring terraces. For high-precision AFM, the noise level of the height measurement is typically 0.3 Å, making it possible to resolve vertical heights as small as 1 Å. It has been shown that, on the $SrTiO_3(111)$ surface, all terraces are separated by integer multiples of 1.12 Å, regardless of the type of reconstruction.[18,27] The surface topography of the same area before and after the photochemical reaction was mapped by AFM operated in tapping mode. The reaction products appeared as brighter contrast compared to the image taken before the reaction. The Gwyddion software package[31] was used to extract height profiles, potential profiles, and to quantify the surface coverage of photochemical reaction product.

XPS spectra measured using Al Kα (1486.6 eV) irradiation (PSP Vacuum Tech, UK) were recorded on annealed $SrTiO_3(111)$ surfaces. To analyze quantitatively the surface chemical composition, high-resolution XPS spectra were taken for Sr 3d, Ti 2p, and O 1s peaks and then analyzed using CasaXPS software.[32] The spectra shown here were acquired with 0.07 eV energy step at 55° off-normal emission. So that the spectra are as representative as possible of the surface used for photochemistry, the crystals were loaded into the vacuum system and analyzed with no further treatment.

3. RESULTS

The surface of the $SrTiO_3(111)$ single crystal substrate after annealing at 1250 °C in air (in the absence of a powder reservoir) is shown in Figure 2a. The terraces formed on the substrate are obvious. The roughness (root-mean-square average of the height profile) of each terrace is less than 1 Å, indicating that they are atomically flat. Figure 2b shows the surface potential image of the same area. When compared to the surface topography, it becomes clear that there are two types of terraces with distinct surface potentials on the $SrTiO_3(111)$ surface. The measured surface potential from KFM (here measured using a TiN coated probe) is affected by the local work function and surface charge. The two types of terraces have KFM potentials that differ by approximately 7 to

DOI: 10.1021/acs.chemmater.6b02205
Chem. Mater. 2016, 28, 5155−5162

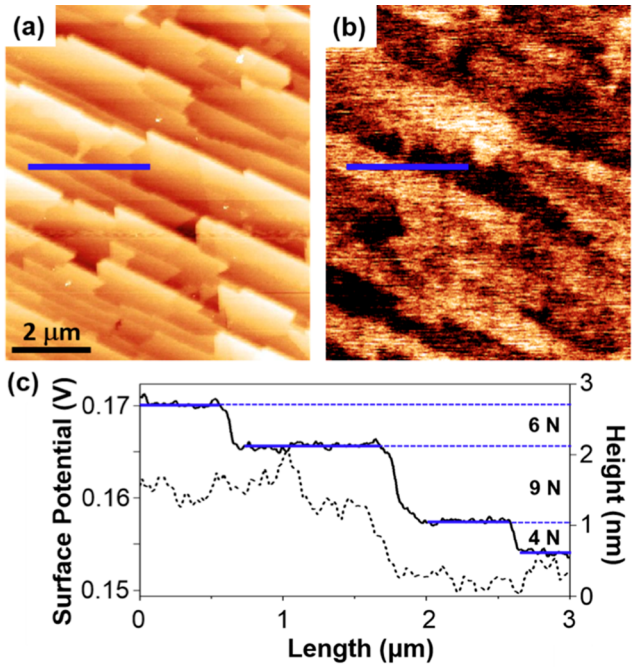

Figure 2. (a) Surface topography AFM image and (b) surface potential image recorded of the same area. Both images are 8 μm × 9.5 μm. The same locations are marked by blue lines in the images. The color range from dark-to-light is (a) 0 to 3 nm, (b) 0.115 to 0.175 V. In panel c, the black solid line is the height cross section at the position of the blue line and the dashed line is potential profile at the same position.

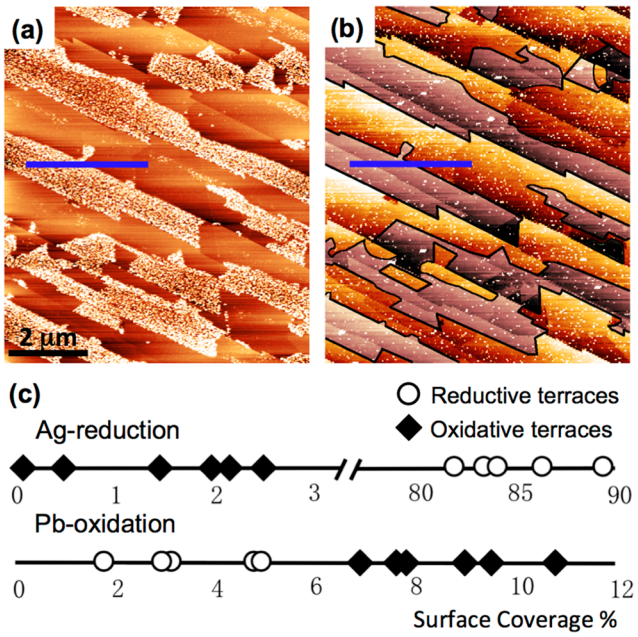

Figure 3. Topographic AFM images of the same area shown in Figure 2, (a) after silver photoreduction and (b) lead photo-oxidation. For comparison, Panel b is segmented using two color saturations. The high color saturation parts include terraces unreactive for photoreduction, and the other parts include terraces reactive for photoreduction. The blue line marks the same position shown in Figure 2. Vertical heights are indicated by the color range which is, from dark-to-light: (a) 0−10 nm and (b) 0−4 nm. In panel c, the fractional surface coverage of Ag and Pb-containing particles on terraces from the low and high saturation parts in panel b are plotted as black diamonds and hollow circles, respectively.

15 mV. The high-precision AFM height profile and the surface potential profile of the lines drawn in Figure 2a,b are plotted as solid and dashed lines, respectively, in Figure 2c. The line crosses four atomically flat terraces. From left to right, the first and second terraces (third and fourth terraces) both have more positive (negative) surface potentials, 0.165 and 0.164 V (0.156 and 0.157 V), respectively, and they are separated by 6.96 Å ≈ 6N (4.49 Å ≈ 4N). As noted before, terraces separated by step heights that are an even multiple of N (N = 1.12 Å) should have the same chemical termination. From the second to third terrace, the chemical termination switches because they are separated by a step of a height that is an odd multiple of N (10.09 Å ≈ 9N); the surface potential also changes to a lower value at this transition.

After the sample was immersed in a silver nitrate (lead acetate) solution and illuminated, new contrast appeared on the surface, corresponding to reduced metallic silver (Pb-containing deposits), as shown in Figure 3a (Figure 3b). The blue line marks the same location as in Figure 2. The fraction of the surface covered by the reaction product on specific terraces is represented in Figure 3c. These two types of terraces behave quite differently for the silver-reduction reaction. Generally, the set of terraces that have a more positive surface potential also have white contrast in Figure 3a. On such terraces, more than 80% of the terrace is covered by Ag after the reaction. Therefore, these terraces are strongly photocathodic. The other terraces, that have more negative potential values, have less than 3% surface coverage.

When the same crystal was used to photo-oxidize Pb^{2+}, the reaction product appears as white dots as shown in Figure 3b. Lead oxidation is a more complex reaction compared to silver reduction. The reaction involves oxygen and the reaction rate is affected by the pH value of the solution.[33,34] The image shows particles on all terraces, but different terraces have noticeably different densities of particles. In Figure 3b, the different terraces have been segmented into two types, indicated by different color saturations. The high color saturation areas only include the set of terraces that are unreactive for the photoreduction of silver (from Figure 3a). The low color saturation areas include the other terraces (the photocathodic terraces reactive for Ag reduction). The terraces with high color (low color) saturation have >6% (<6%) of the surface covered by Pb-containing particles, which means that high color (low color) saturation terraces are more (less) reactive for photo-oxidation reactions.

The results in Figure 3 show that complementary photochemical reactions occur preferentially on distinct terraces on the $SrTiO_3$(111) surface. One set of terraces is reactive for the photoreduction of silver and is less reactive for the photo-oxidation of lead; these terraces are referred to here as photocathodic. The other set of terraces is more reactive for photo-oxidation and is nearly unreactive for the photoreduction of silver; these terraces are referred to here as photoanodic. Moreover, when correlated with Figure 2b, photocathodic terraces have a relatively higher surface potential, whereas photoanodic terraces have a relatively lower surface potential.

Three more pieces of $SrTiO_3$(111) crystals were annealed in the same combustion boat, but with 2 g of $TiO_2/SrTiO_3$ powder mixtures surrounding (but not in contact with) the crystal. The topographic AFM images in Figure 4 compare the ability of surfaces to photochemically reduce silver after they

DOI: 10.1021/acs.chemmater.6b02205
Chem. Mater. 2016, 28, 5155−5162

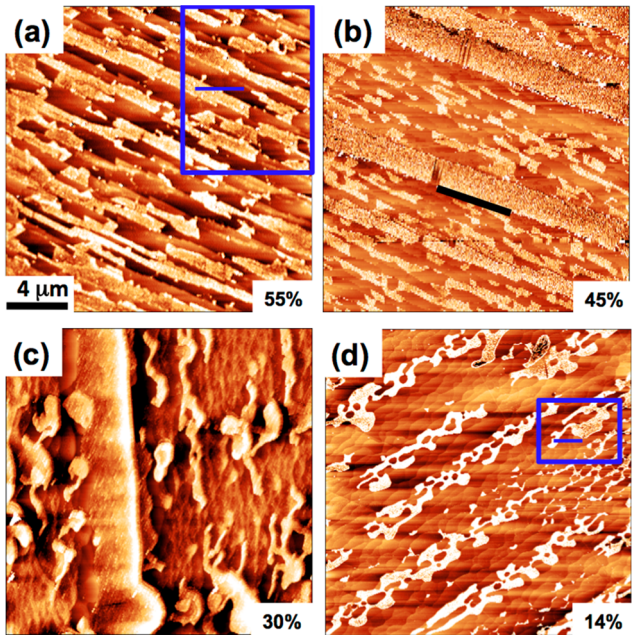

Figure 4. Topographic AFM images of samples annealed without (a) and with (b–d) different $TiO_2/SrTiO_3$ powder mixtures after the photochemical reduction of silver. Heated with (a) no powder, (b) 31.4 wt % Ti, (c) 36.4 wt % Ti, and (d) 60.0 wt % Ti. All images are 20 μm × 20 μm laterally and the dark-to-light vertical scales are all 0–10 nm. The blue boxes and blue lines in panel a (and panel d) indicate the areas from which the high-precision AFM images presented in Figure 2 (Figure 5) were recorded. The black line in panel b marks the same location that is marked in Figure S1b and Figure S2. The fractional coverage of photocathodic terraces in each image is marked in the lower right corner of each image.

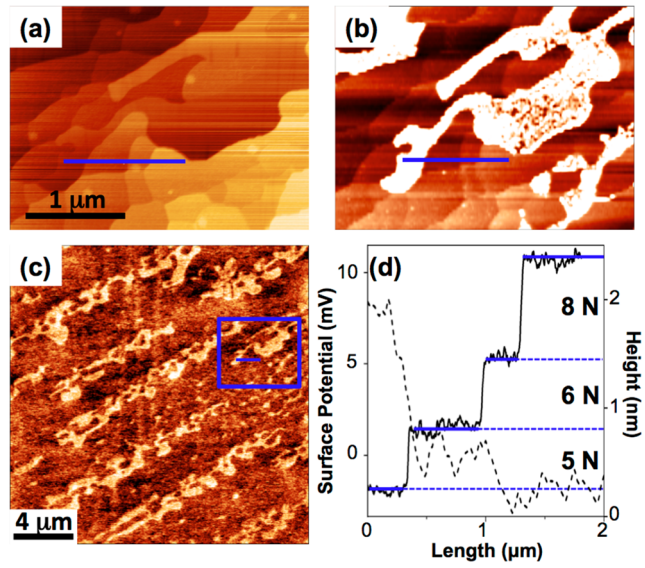

Figure 5. (a) High precision topographic AFM image recorded on the clean surface of a sample annealed with TiO_2 powder. The field of view is 3 μm × 3.7 μm. (b) Image of the same area after the photoreduction of silver. (c) The surface potential image of the area shown in Figure 4(d). The field of view is 20 μm × 20 μm. (d) The height (solid line) and surface potential (dashed line) profiles from the location of the blue line in (a) and (c). The dark-to-light vertical contrast is (a): 0–4 nm, (b): 0–10 nm, (c) −6–10 mV.

were annealed with (a) no excess powder, (b) 31.4 wt % Ti powder (TiO_2:$SrTiO_3$ = 3:7), (c) 36.4 wt % Ti powder (TiO_2:$SrTiO_3$ = 1:1), and (d) 60 wt % Ti powder (pure TiO_2). Each sample was exposed to light for the same amount of time in a solution with the same concentration of silver. The area shown in Figure 4a contains the area already shown in Figure 2 and Figure 3 (enclosed by the blue box). For this control sample, the photocathodic terraces, covered by silver, make up about 55% of the area. An AFM image of the sample annealed in a $TiO_2/SrTiO_3$ powder mixture with a Ti concentration of 31.4 wt % is shown in Figure 4b. About 45% of the area is covered by silver particles after silver-reduction. An AFM image of the sample annealed with a $TiO_2/SrTiO_3$ powder mixture with 36.4 wt % Ti is shown in Figure 4c. For this sample, about 30% of the area is covered by silver particles after silver-reduction. An AFM image of the sample annealed with 60.0 wt % Ti (i.e., pure TiO_2 powder) is shown in Figure 4d. For this sample, only 14% of the surface is reactive for silver reduction. Note that, as the excess Ti concentration in the powder increases, the shape of the terraces also changes from straight edges to curved edges. A clearer view of the changes in terrace shape is observable in Figure S1, showing AFM images of the same areas, but without the reaction product.

To exclude the possibility that a new phase is formed on the surface of the crystals annealed with excess powder, step height and KFM measurement were repeated on the sample annealed with pure TiO_2 powder. The high-precision topographic AFM image shown in Figure 5a was recorded in the area denoted by the blue box in Figure 4d (but on the clean surface). A topographic AFM image of the same location after the photoreduction of silver is shown in Figure 5b. A KFM image (mapped with a Pt/Cr coated probe) of the clean surface, in the same area that is shown in Figure 4d, is shown in Figure 5c. From the KFM image, we can clearly see that, similar to the observations from the sample annealed without powder, there are still two distinct contrast levels with a potential difference of 7 to 15 mV. Note that the absolute value of the surface potential changed from the 155 to 175 mV range (Figure 2c) to the −5 to +15 mV range (Figure 5d); this is because the AFM probe was coated with a different metal with a different work function. After comparing the pattern of silver reduced on the surface in Figure 4d with the potential contrast in Figure 5c, there is a clear correlation between surface potential and the photochemical reactivity. All photocathodic terraces have more positive potentials than the photoanodic terraces, as described previously.

The height and surface potential profile along the line drawn in Figure 5a,d are extracted and plotted in Figure 5c. The line crosses four terraces. From left to right, the first terrace was reactive for photoreduction according to the silver pattern, and the following three terraces were unreactive. As noted before, terraces separated by step heights of an even multiple of N (= 1.12 Å) should have the same reactivity, and terraces separated by step heights equal to an odd multiple of N should have different reactivities. From left to right, the average heights of each terrace are 2.34, 8.19, 14.71, and 23.61 Å. Therefore, the step height between the first and second terrace is 5.85 Å ≈ 5N, and the reactivity and surface potential both changed at this transition. The step heights between the second and third terraces and the third and fourth terraces are 6.52 Å (6N) and 8.9 Å (8N), respectively, and all three of these terraces are unreactive for the photoreduction of silver and have less positive potentials. The height profiles of five more lines were

DOI: 10.1021/acs.chemmater.6b02205
Chem. Mater. 2016, 28, 5155–5162

extracted from other locations and the step heights are all correlated with changes in reactivity and surface potential.

Experiments were also conducted to test the KFM measurement's sensitivity to the experimental conditions (see Figure S2). We compared the contrast in KFM images of surfaces immediately after annealing with the contrast in images recorded after the surface was used to photochemically reduce silver and that silver was removed. The comparison indicates that the distribution of the potential on the surface is the same before and after the photochemical reaction. When KFM images were recorded after a 20 h water immersion, the contrast between two types of terraces was weakened, but the characteristics did not change. When KFM images of a sample recorded immediately after annealing were compared to those recorded after storing the sample in air for 6 months, the contrast was the same. Not only are the surface potential measurements stable after all of these treatments, the photochemical reactions can also be reproduced after different steps in the characterization and repeated cleaning processes. The fact that the surface properties are not changed by these treatments suggests that that chemical state of the surface (including hydration), is established by the original annealing treatment, and is stable for at least months in air and hours in aqueous solutions.

To explore how the elemental ratios of Sr, Ti, and O vary on surfaces annealed in different conditions, we used XPS to compare the surface chemistries of samples that are majority (55%) photocathodic and majority (86%) photoanodic. We note that the spectra were recorded on samples without any in vacuum treatments to remove surface contamination. Therefore, the absolute concentrations of elements on the surface are not expected to be accurate. However, we assume the differences between the majority photoanodic and photocathodic surfaces are a meaningful measure of the relative concentration of Ti on the two surfaces. High-resolution XPS was used to measure the Sr 3d and Ti 2p spectra. The Sr/Ti atomic ratio was determined from the ratio of the integrated intensities of the Sr 3d and Ti 2p peaks.[17,35] We compared the sample heated with no powder (the majority photocathodic sample shown in Figure 4a) and the one heated with pure TiO_2 powder (the majority photoanodic samples shown in Figure 4d). The spectra for these samples are shown in Figure 6.

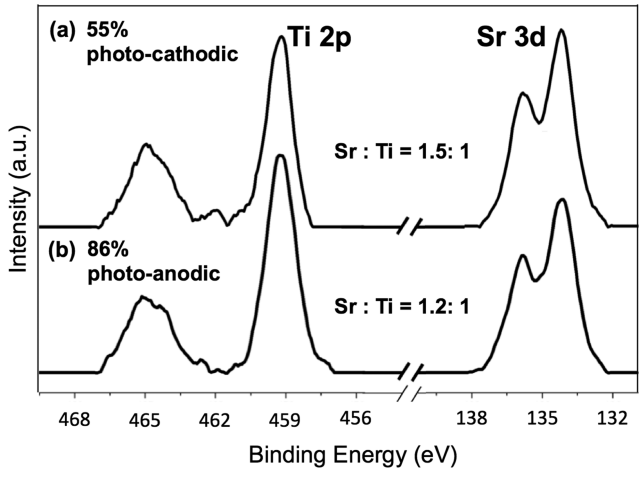

Figure 6. Ti 2p and Sr 3d core level XPS spectra from $SrTiO_3(111)$ surfaces with (a) 55% photocathodic terraces and (b) 86% photoanodic terraces.

Consistent with previous reports,[17] the Sr/Ti ratios are consistently greater than one. The sample annealed with no powder and a 55% photocathodic surface has a Sr/Ti ratio of 1.5. The sample annealed with TiO_2 powder and an 86% photoanodic surface has a Sr/Ti ratio of 1.2. On the basis of this comparison, when the sample was annealed in the presence of excess TiO_2 powder, the surface averaged Sr/Ti ratio, surface potential, and photocathodic reactivity are all lower, whereas the photoanodic reactivity is higher. Therefore, high-temperature anneals in the presence of Sr- and Ti-containing powder reservoirs having stoichiometries different from $SrTiO_3$ can lead to modifications of the overall composition of the $SrTiO_3(111)$ single crystal surface.

The presence of hydroxyls on the surfaces was also verified by the XPS spectra of the O 1s peaks, as shown in Figure 7.

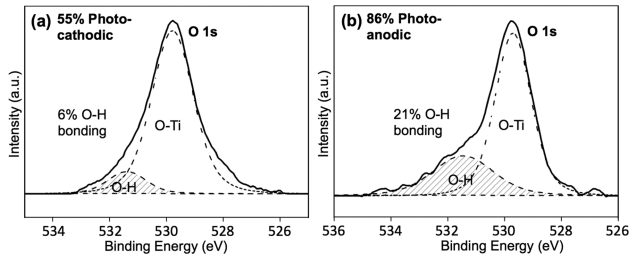

Figure 7. Oxygen 1s XPS spectra from $SrTiO_3(111)$ surfaces with (a) 55% photocathodic terraces and (b) 86% photoanodic terraces.

The main O 1s peak at 529.8 eV is ascribed to the Ti−O bonding and the second oxygen peak (the shaded area in Figure 7) at 531.7 eV belongs to the hydroxyl species. The sample with the more photocathodic surface had 6% oxygen bonded in the O−H state at surface whereas the more photoanodic surface has 21%, relative to the total O 1s signal. These adsorbed species are likely to reduce the charge that is on the bare surfaces and affect the measured potential in the KFM images.

4. DISCUSSION

The results presented here show that $SrTiO_3(111)$ surfaces annealed at 1250 °C exhibit two types of terraces that have distinct surface potentials in KFM images. The two types of terraces also have distinct photochemical properties: the terrace with the more positive surface potential is photocathodic and promotes reduction, while the terrace with the less positive surface potential is photoanodic and promotes oxidation. These observations are consistent with what has been observed on the surfaces of the polar domains of ferroelectrics,[18,36] thin films supported by ferroelectrics,[37−39] ferroelastic materials,[12,40] and on Fe_2O_3 polycrystals.[41] In all cases, surfaces with a more positive potential have reduced upward (or increased downward) band bending at the surface. Therefore, it is easier for photogenerated electrons to reach the surface and participate in photoreduction reactions. For terraces with a less positive surface potential, increased upward band bending prevents electrons from getting to the surface while holes are driven "uphill" and can participate in oxidation reactions. The observation that some oxidation product appears on the more positive, photocathodic terraces suggests that the bands are still bent upward on these surfaces, but not far enough to prevent reduction reactions from occurring. This line of

DOI: 10.1021/acs.chemmater.6b02205
Chem. Mater. 2016, 28, 5155−5162

argument has been supported quantitatively through simulations of thin films supported by ferroelectrics.[42]

After measuring the step heights between terraces on clean surfaces, it was determined that terraces of similar reactivity and surface potential were separated by even multiples of the spacing between lattice planes (even-N, N = 1.12 Å) that preserve the composition of the termination layer, whereas terraces of different reactivity were separated by odd-N distances that change the composition of the termination layer. As mentioned before, all terraces, regardless of the type of reconstruction present, are separated by integer multiples of 1.12 Å for $SrTiO_3(111)$.[18,25] According to the model of the ideal, unreconstructed $SrTiO_3(111)$ surface (illustrated in Figure 1b), the Ti and SrO_3 terminated surfaces have formal charges of +4 and −4, respectively. However, real terraces are unlikely to have these compositions and charges. Analysis of the $SrTiO_3(111)$ surfaces using experiments such as mass spectroscopy of recoiled ions and coaxial impact-collision ion scattering spectroscopy lead to the conclusion that the surface in a vacuum is Ti-rich,[23] or terminated by TiO_x layers.[25,43,44] When heated in vacuum, it has been shown that the $SrTiO_3(111)$ surface reconstructs into a variety of Ti-rich structures with $(n \times n)$ repeat units, with $2 \leq n \leq 6$.[15] The high temperature annealing used in the present experiments may have also led to surface modifications, but not necessarily those that have been observed in a vacuum.

For $SrTiO_3$ in aqueous solutions, the surfaces are covered with adsorbates, such as OH^-. For example, it has been reported that H_2O and O_2 chemisorb on the reduced $SrTiO_3(111)$ surface terminated by Ti^{3+}.[16] When irradiated with band gap light in vacuum, oxygen has been reported to photodesorb from the surface. However, illumination also increases the concentration of surface hydroxyls. Here, we have found that the photoanodic surface has more hydroxyls than the photocathodic surface. This likely affects the surface charge and the measured potential in the KFM images.

The work function of the ideal Ti^{4+} termination is calculated to be 0.6 eV greater than the work function of the ideal SrO_3^{4+} termination.[43] The differences in the work functions of various TiO_x and SrO_x reconstructed surfaces are calculated to fall in the range of 0.3 to 0.8 eV and, in all cases, the TiO_x termination has a larger work function than the SrO_x termination.[19] These values are obviously larger than any of the potential differences that we measure with KFM. This is not surprising for measurements made in the ambient. For example, we regularly set up the instrument using a Pt−Au calibration standard. Although these two metals have a work function difference of 0.6 eV, the difference in potential measured by ambient KFM is in the range of 20 to 30 mV. This reduction in measured potential difference is similar in magnitude to the difference we observe on the photoanodic and photocathodic terraces (about 10 mV). Measurements of the $SrTiO_3$ (100) surface in a vacuum with mixed terminations have also shown that there are potential differences between terraces of different termination (on the order of tens of mV), and that the actual difference was very sensitive the surface preparation and Sr concentration.[20] All of these calculations and observations are consistent with the evidence presented here that terraces on the $SrTiO_3(111)$ surface with different compositions have different potentials.

The reconstruction of the surface and the adsorption of charged species are thought to influence photochemical reactions on other oxides, such as hematite. Hematite's structure indicates its $(1\bar{2}10)$ prismatic plane is polar terminated and its $(1\bar{1}02)$ rhombohedral plane is charge neutral. However, KFM images of air-annealed hematite show that the $(1\bar{2}10)$ plane has a very different surface potential and is the most reactive orientation for silver-reduction. The unexpected high surface potential on Fe_2O_3 $(1\bar{1}02)$ may be caused by adsorbed hydroxyl species and possibly surface reconstructions.[41] That the surface potential and reactivity are correlated on both the single crystal terraces and averaged over individual grains of polycrystals implies that these observations are a potentially generic avenue toward controlling spatially selective reactivity in photocatalysts.

Controlling the surface termination of a single crystal of $SrTiO_3$ using a reservoir of powders represents a straightforward and complementary method to vacuum annealing and solution chemical treatments developed for surface engineering thin film substrates[21−24] for improved film growth.[25,45] This process must work through a vapor phase interaction between the crystal surface and the powder reservoir during the annealing treatments, which results in a controllable modification in the ratio of photocathodic to photoanodic terraces. At these temperatures, the vapor pressure of titania is negligible. However, the vapor pressure of SrO is measurable[46] and the presence of water vapor converts strontium oxide to a hydroxide that has a vapor pressure which is larger by many orders of magnitude.[47] Therefore, the most likely explanation for the influence of the powder reservoir on the surface termination is that SrO vapor in the furnace reacts with excess titania in the powder bed and sets up a concentration gradient for the transport of the SrO. This is consistent with the observation that as the TiO_2 concentration in the powder bed increases, the surfaces are increasingly depleted of Sr (the Sr:Ti intensity in XPS decreases). This is also consistent with a report showing that Sr in $SrTiO_3$ evaporates at high temperature.[48]

The control of the ratio of photocathodic to photoanodic sites on separate terraces has the potential to impact the development of photocatalysts for water-splitting. Water-splitting using suspended oxide particles has been determined to have a lower cost than photoelectrochemical cells (PECs).[49] Compared to PECs, the overall quantum efficiency of powders is lower, mainly because of the constraint that both of the redox reactions must occur on the same surface and at the same potential. In such a case, the slowest of the two half reactions will determine the overall reaction rate. The overall rate will be maximized when the net oxidation and net reduction reactions occur at the same rate. Therefore, the ideal particle would have the appropriate ratio of photocathodic and photoanodic terraces to maximize the reaction rate. The spatial separation of the terraces would have the additional benefit of suppressing the back reaction of intermediate species. The fact that the ratio of oxidizing to reducing sites can be controlled and that they are stable, suggests that it will be possible to optimize the surface structure of photocatalyst particles using procedures similar to those described here.

5. CONCLUSIONS

$SrTiO_3(111)$ surfaces annealed in air exhibit two types of terraces with distinct surface potentials. The different types of terraces are separated by odd integer multiples of the interplanar spacing, corresponding to different chemical terminations of the bulk crystal. The terraces with the more positive (less positive) surface potential have photocathodic (photoanodic) surface properties. The different types of terraces exhibit different photochemical activities for oxidation

DOI: 10.1021/acs.chemmater.6b02205
Chem. Mater. 2016, 28, 5155−5162

or reduction reactions, which can be rationalized by considering which photogenerated carrier is attracted to the terrace based on surface potentials. The relative surface coverage of a specific type of terrace, and the surface reactivity, can be controlled by annealing the crystal in the presence of reservoirs of TiO_2/$SrTiO_3$ powders. The concentration of titanium at the surface increases with the fraction of TiO_2 in the powder reservoir, as does the fraction of photoanodic terraces. The relative area of photoanodic terraces can be manipulated through this method, and we demonstrate control within the range of 45% to 86% of the total area.

■ ASSOCIATED CONTENT

Supporting Information

The Supporting Information is available free of charge on the ACS Publications website at DOI: 10.1021/acs.chemmater.6b02205.

Results of additional supporting experiments (PDF).

■ AUTHOR INFORMATION

Corresponding Author

*Gregory S. Rohrer, Department of Materials Science and Engineering, Carnegie Mellon University, 5000 Forbes Ave., Pittsburgh, PA 15213-3890, gr20@andrew.cmu.edu.

Funding

National Science Foundation grant DMR 1206656, CMU Grant MCF-677785.

Notes

The authors declare no competing financial interest.

■ ACKNOWLEDGMENTS

The authors acknowledge the support of National Science Foundation grant DMR 1206656. The authors acknowledge use of the Materials Characterization Facility at Carnegie Mellon University supported by grant MCF-677785. The authors thank Y. Wei and M. Skowronski for assistance with the XPS measurements.

■ REFERENCES

(1) Han, F.; Kambala, V. S. R.; Srinivasan, M.; Rajarathnam, D.; Naidu, R. Tailored titanium dioxide photocatalysts for the degradation of organic dyes in wastewater treatment: A review. *Appl. Catal., A* **2009**, *359* (1−2), 25−40.

(2) Hoffmann, M. R.; Martin, S. T.; Choi, W. Y.; Bahnemann, D. W. Environmental applications of semiconductor photocatalysts. *Chem. Rev.* **1995**, *95* (1), 69−96.

(3) Kitano, M.; Hara, M. Heterogeneous photocatalytic cleavage of water. *J. Mater. Chem.* **2010**, *20* (4), 627−641.

(4) Kudo, A.; Miseki, Y. Heterogeneous photocatalyst materials for water splitting. *Chem. Soc. Rev.* **2009**, *38* (1), 253−278.

(5) Osterloh, F. E. Inorganic nanostructures for photoelectrochemical and photocatalytic water splitting. *Chem. Soc. Rev.* **2013**, *42* (6), 2294−2320.

(6) Osterloh, F. E.; Parkinson, B. A. Recent developments in solar water-splitting photocatalysis. *MRS Bull.* **2011**, *36* (1), 17−22.

(7) Batzill, M. Fundamental aspects of surface engineering of transition metal oxide photocatalysts. *Energy Environ. Sci.* **2011**, *4* (9), 3275−3286.

(8) Kakekhani, A.; Ismail-Beigi, S. Ferroelectric-Based Catalysis: Switchable Surface Chemistry. *ACS Catal.* **2015**, *5* (8), 4537−4545.

(9) Li, L.; Salvador, P. A.; Rohrer, G. S. Photocatalysts with internal electric fields. *Nanoscale* **2014**, *6* (1), 24−42.

(10) Li, L.; Rohrer, G. S.; Salvador, P. A. Heterostructured Ceramic Powders for Photocatalytic Hydrogen Production: Nanostructured TiO_2 Shells Surrounding Microcrystalline (Ba,Sr)TiO_3 Cores. *J. Am. Ceram. Soc.* **2012**, *95* (4), 1414−1420.

(11) Li, L.; Zhang, Y. L.; Schultz, A. M.; Liu, X.; Salvador, P. A.; Rohrer, G. S. Visible light photochemical activity of heterostructured $PbTiO_3$-TiO_2 core-shell particles. *Catal. Sci. Technol.* **2012**, *2* (9), 1945−1952.

(12) Munprom, R.; Salvador, P. A.; Rohrer, G. S. Ferroelastic domains improve photochemical reactivity: a comparative study of monoclinic and tetragonal $(Bi_{1-0.5x}Na_{0.5x})(V_{1-x}Mo_x)O_4$ ceramics. *J. Mater. Chem. A* **2016**, *4* (8), 2951−2959.

(13) Lehn, J. M.; Sauvage, J. P.; Ziessel, R. Photochemical water splitting continuous generation of hydrogen and oxygen by irradiation of aqueous suspensions of metal loaded strontium-titanate. *New J. Chem.* **1980**, *4* (11), 623−627.

(14) Townsend, T. K.; Browning, N. D.; Osterloh, F. E. Nanoscale Strontium Titanate Photocatalysts for Overall Water Splitting. *ACS Nano* **2012**, *6* (8), 7420−7426.

(15) Russell, B. C.; Castell, M. R. Surface of sputtered and annealed polar $SrTiO_3$(111): TiO_x-rich (*n* x *n*) reconstructions. *J. Phys. Chem. C* **2008**, *112* (16), 6538−6545.

(16) Ferrer, S.; Somorjai, G. A. UPS and XPS studies of chemisorption of O_2, H_2, and H_2O on reduced and stoichiometric $SrTiO_3$(111) surfaces - the effects of illumination. *Surf. Sci.* **1980**, *94* (1), 41−56.

(17) Nagarkar, P. V.; Searson, P. C.; Gealy, F. D. Effect of surface-treatment on $SrTiO_3$ - an X-ray photoelectron spectroscopic study. *J. Appl. Phys.* **1991**, *69* (1), 459−462.

(18) Giocondi, J. L.; Rohrer, G. S. Structure sensitivity of photochemical oxidation and reduction reactions on $SrTiO_3$ surfaces. *J. Am. Ceram. Soc.* **2003**, *86* (7), 1182−1189.

(19) Pojani, A.; Finocchi, F.; Noguera, C. Polarity on the $SrTiO_3$ (111) and (110) surfaces. *Surf. Sci.* **1999**, *442* (2), 179−198.

(20) Aballe, L.; Matencio, S.; Foerster, M.; Barrena, E.; Sanchez, F.; Fontcuberta, J.; Ocal, C. Instability and Surface Potential Modulation of Self-Patterned (001)$SrTiO_3$ Surfaces. *Chem. Mater.* **2015**, *27* (18), 6198−6204.

(21) Doan, T. D.; Giocondi, J. L.; Rohrer, G. S.; Salvador, P. A. Surface engineering along the close-packed direction of $SrTiO_3$. *J. Cryst. Growth* **2001**, *225* (2−4), 178−182.

(22) Sigmund, W. M.; Rotov, M.; Jiang, Q. D.; Brunen, J.; Zegenhagen, J.; Aldinger, F. A titanium-rich (111) surface of $SrTiO_3$ single crystals by thermal annealing. *Appl. Phys. A: Mater. Sci. Process.* **1997**, *64* (2), 219−220.

(23) Biswas, A.; Rossen, P. B.; Yang, C. H.; Siemons, W.; Jung, M. H.; Yang, I. K.; Ramesh, R.; Jeong, Y. H. Universal Ti-rich termination of atomically flat $SrTiO_3$ (001), (110), and (111) surfaces. *Appl. Phys. Lett.* **2011**, *98* (5), 051904.

(24) Chang, J.; Park, Y.-S.; Kim, S.-K. Atomically flat single-terminated $SrTiO_3$ (111) surface. *Appl. Phys. Lett.* **2008**, *92* (15), 152910.

(25) Hallsteinsen, I.; Nord, M.; Bolstad, T.; Vullum, P.-E.; Boschker, J. E.; Longo, P.; Takahashi, R.; Holmestad, R.; Lippmaa, M.; Tybell, T. Effect of Polar (111)-Oriented $SrTiO_3$ on Initial Perovskite Growth. *Cryst. Growth Des.* **2016**, *16* (4), 2357−2362.

(26) Dunn, S.; Jones, P. M.; Gallardo, D. E. Photochemical growth of silver nanoparticles on c^- and c^+ domains on lead zirconate titanate thin films. *J. Am. Chem. Soc.* **2007**, *129* (28), 8724−8728.

(27) Giocondi, J. L.; Rohrer, G. S. Spatial separation of photochemical oxidation and reduction reactions on the surface of ferroelectric $BaTiO_3$. *J. Phys. Chem. B* **2001**, *105* (35), 8275−8277.

(28) Li, R.; Zhang, F.; Wang, D.; Yang, J.; Li, M.; Zhu, J.; Zhou, X.; Han, H.; Li, C. Spatial separation of photogenerated electrons and holes among {010} and {110} crystal facets of $BiVO_4$. *Nat. Commun.* **2013**, *4*, 1432.

(29) Lowekamp, J. B.; Rohrer, G. S.; Hotsenpiller, P. A. M.; Bolt, J. D.; Farneth, W. E. Anisotropic photochemical reactivity of bulk TiO_2 crystals. *J. Phys. Chem. B* **1998**, *102* (38), 7323−7327.

DOI: 10.1021/acs.chemmater.6b02205
Chem. Mater. 2016, 28, 5155−5162

(30) Munprom, R.; Salvador, P. A.; Rohrer, G. S. The orientation dependence of the photochemical reactivity of $BiVO_4$. *J. Mater. Chem. A* **2015**, *3* (5), 2370−2377.
(31) Gwyddion; http://gwyddion.net/resources.php, 2011.
(32) Fairley, N. CasaXPS VAMAS processing software; http://www.casaxps.com, 2010.
(33) Tanaka, K.; Harada, K.; Murata, S. Photocatalytic deposition of metal-ions onto TiO_2 powder. *Sol. Energy* **1986**, *36* (2), 159−161.
(34) Torres, J.; Cerveramarch, S. Kinetics of the photoassisted catalytic-oxidation of Pb(II) in TiO_2 suspensions. *Chem. Eng. Sci.* **1992**, *47* (15−16), 3857−3862.
(35) Hikita, T.; Hanada, T.; Kudo, M.; Kawai, M. Structure and electronic state of the TiO_2 and SrO terminated $SrTiO_3$(100) surfaces. *Surf. Sci.* **1993**, *287*, 377−381.
(36) Schultz, A.; Zhang, Y.; Salvador, P.; Rohrer, G. Effect of Crystal and Domain Orientation on the Visible-Light Photochemical Reduction of Ag on $BiFeO_3$. *ACS Appl. Mater. Interfaces* **2011**, *3* (5), 1562−1567.
(37) Burbure, N. V.; Salvador, P. A.; Rohrer, G. S. Photochemical Reactivity of Titania Films on $BaTiO_3$ Substrates: Origin of Spatial Selectivity. *Chem. Mater.* **2010**, *22* (21), 5823−5830.
(38) Burbure, N. V.; Salvador, P. A.; Rohrer, G. S. Photochemical Reactivity of Titania Films on $BaTiO_3$ Substrates: Influence of Titania Phase and Orientation. *Chem. Mater.* **2010**, *22* (21), 5831−5837.
(39) Zhang, Y. L.; Schultz, A. M.; Salvador, P. A.; Rohrer, G. S. Spatially selective visible light photocatalytic activity of TiO_2/$BiFeO_3$ heterostructures. *J. Mater. Chem.* **2011**, *21* (12), 4168−4174.
(40) Munprom, R.; Salvador, P. A.; Rohrer, G. S. Polar Domains at the Surface of Centrosymmetric $BiVO_4$. *Chem. Mater.* **2014**, *26* (9), 2774−2776.
(41) Zhu, Y.; Schultz, A. M.; Rohrer, G. S.; Salvador, P. A. The Orientation Dependence of the Photochemical Activity of α-Fe_2O_3. *J. Am. Ceram. Soc.* **2016**, *99*, 2428−2435.
(42) Glickstein, J. J.; Salvador, P. A.; Rohrer, G. S. A Computational Model of Domain Specific Reactivity on Coated Ferroelectric Photocatalysts. *J. Phys. Chem. C* **2016**, *120* (23), 12673−12684.
(43) Chiaramonti, A. N.; Lanier, C. H.; Marks, L. D.; Stair, P. C. Time, temperature, and oxygen partial pressure-dependent surface reconstructions on $SrTiO_3$(111): A systematic study of oxygen-rich conditions. *Surf. Sci.* **2008**, *602* (18), 3018−3025.
(44) Marks, L. D.; Chiaramonti, A. N.; Tran, F.; Blaha, P. The small unit cell reconstructions of $SrTiO_3$(111). *Surf. Sci.* **2009**, *603* (14), 2179−2187.
(45) Blok, J. L.; Wan, X.; Koster, G.; Blank, D. H. A.; Rijnders, G. Epitaxial oxide growth on polar (111) surfaces. *Appl. Phys. Lett.* **2011**, *99* (15), 151917.
(46) Lamoreaux, R. H.; Hildenbrand, D. L.; Brewer, L. High-temperature vaporization behavior of oxides 2. Oxides of Be, Mg, Ca, Sr, Ba, B, Al, Ga, In, Tl, Si, Ge, Sn, Pb, Zn, Cd, and Hg. *J. Phys. Chem. Ref. Data* **1987**, *16* (3), 419−443.
(47) Zhang, T.; Wang, S. Seals for Planar Solid Oxide Fuel Cells: The State of the Art. In *Nanostructured and Advanced Materials for Fuel Cells*; Jiang, S. P., Shen, P. K., Eds.; CRC Press, Taylor Francis Group: Boca Raton, FL, 2008; p 58.
(48) Wang, Z.; Yang, F.; Zhang, Z.; Tang, Y.; Feng, J.; Wu, K.; Guo, Q.; Guo, J. Evolution of the surface structures on $SrTiO_3$(110) tuned by Ti or Sr concentration. *Phys. Rev. B: Condens. Matter Mater. Phys.* **2011**, *83* (15), 155453.
(49) Sathre, R.; Scown, C. D.; Morrow, W. R., III; Stevens, J. C.; Sharp, I. D.; Ager, J. W., III; Walczak, K.; Houle, F. A.; Greenblatt, J. B. Life-cycle net energy assessment of large-scale hydrogen production via photoelectrochemical water splitting. *Energy Environ. Sci.* **2014**, *7* (10), 3264−3278.

DOI: 10.1021/acs.chemmater.6b02205
Chem. Mater. 2016, 28, 5155−5162